

Investigation of Product Accuracy as a Function of Input and Model Uncertainties: Case Study with SeaWiFS and MODIS LAI/FPAR Algorithm

Yujie Wang¹, Yuhong Tian¹, Yu Zhang¹, Nazmi El-Saleous²,
Yuri Knyazikhin¹, Eric Vermote², and Ranga B. Myneni¹

¹Department of Geography, Boston University, Boston, MA 02215, USA

²NASA Goddard Space Flight Center, Code 922, Greenbelt, MD 20771, USA

Correspondence

Yujie Wang

Department of Geography, Boston University
675 Commonwealth Avenue, Boston, MA, 02215, USA

email: yjwang@bu.edu

telephone: 617-353-8342

fax: 617-353-8399

Submitted for publication in *Remote Sensing of Environment*

Submitted 10 June, 2001, Revised 20 Feb., 2001

ABSTRACT

The derivation of vegetation leaf area index (LAI) and the fraction of photosynthetically active radiation (FPAR) absorbed by vegetation globally from the Sea-Viewing Wide Field-of-view Sensor (SeaWiFS) multispectral surface reflectances using the algorithm developed for the MODIS (moderate resolution imaging spectroradiometer) instrument is discussed here, with special emphasis on the quality of the retrieved fields. Uncertainties in the land surface reflectance and model used in the algorithm determine the quality of the retrieved LAI/FPAR fields. The in-orbit radiances measured by space-borne sensors require corrections for calibration and atmospheric effects and this introduces uncertainty in the surface reflectance products. The model uncertainty characterizes the accuracy of a vegetation radiation interaction model to approximate the observed variability in surface reflectances. When the amount of spectral information input to the retrieval technique is increased, not only does this increase the overall information content but also decreases the summary accuracy in the data. The former enhances quality of the retrievals, while the latter suppresses it. The quality of the retrievals can be influenced by the use of uncertainty information in the retrieval technique. We introduce a stabilized uncertainty which is basic information to the retrieval technique required to establish its convergence; that is, the more the measured information and the more accurate this information is, the more reliable and accurate the algorithm output will be. The quality of retrieval is a function of the stabilized uncertainty whose accurate specification is critical for deriving biophysical surface parameters of the highest quality possible using multispectral land surface data. The global LAI and FPAR maps derived from SeaWiFS multispectral surface reflectances and uncertainty information as well as an analysis of these products is presented here.

INTRODUCTION

Leaf area index (LAI) and the fraction of photosynthetically active radiation absorbed by vegetation (FPAR) which characterize vegetation canopy functioning and its energy absorption capacity are important variables in terrestrial modeling studies of canopy photosynthesis and transpiration. Terrestrial carbon exchange studies with the retrieved structural information show that canopy and landscape structure plays a major role in determining CO₂ fluxes in spatially heterogeneous environments (Sellers et al., 1997). Therefore, these variables are key state parameters in most ecosystem productivity models and in global models of climate, hydrology, biogeochemistry and ecology (Sellers et al., 1996). Advances in remote sensing technology (Deschamps et al., 1994; Justice et al., 1998; Diner et al., 1999) and radiative transfer modeling (Ross and Marshak, 1984; Kuusk, 1985; Verstraete et al., 1990; Myneni, 1991; Ross et al., 1992; Kimes et al., 2000) greatly improved the possibility of accurate estimates of biophysical information from spatial, spectral, angular and temporal resolution of remotely sensing data. The objective of this paper is to demonstrate that uncertainties in multispectral surface reflectances are critical input information to retrieval algorithms in order to derive biophysical surface parameters of the highest quality possible using multispectral land surface data. The operational algorithm for the production of global LAI and FPAR fields developed for the MODIS (moderate resolution imaging spectroradiometer) instrument applied to the SeaWiFS (Sea-Viewing Wide Field-of-view Sensor) data is used to demonstrate this technique.

At least two factors influence the quality of surface biophysical parameters retrieved from remotely sensed surface reflectances:

- uncertainty in the land surface reflectance product. Satellite-borne sensors measure in-orbit radiances of the target through the atmosphere. The surface reflectances are obtained by processing the in-orbit data to correct for atmospheric and other environmental effects which leads to uncertainties in the surface reflectance product;
- model uncertainty determined by the range of natural variation in biophysical parameters not accounted by the model. In general, this type of uncertainty depends on the amount of information available when retrieving biophysical parameters from surface reflectances as well as the temporal and spatial resolution of data (Diner et. al., 1999).

In general, these uncertainties set a limit to the quality of retrievals; that is, accuracy in the retrievals cannot be better than summary accuracy in data and the model. However, the quality of the retrievals can be influenced by the use of uncertainty information in the retrieval technique. Definitions of uncertainties in the land surface reflectance product and model, as well as their impact on the retrievals, are discussed in the third section following a formulation of the inverse problem of retrieving LAI and FPAR from surface spectral reflectances. It is shown that if uncertainties are ignored, it can result not only in the loss of information conveyed by the multispectral data, but also in destabilization of the retrieval process. Results from this section underlie our strategy of producing global SeaWiFS LAI/FPAR fields of highest possible quality.

FORMULATION OF THE INVERSE PROBLEM

The problem of retrieving LAI and FPAR from atmospherically corrected Bi-directional Reflectance Distribution Function (BRDF) is formulated as follows (Knyazikhin et al., 1998a):

given sun (Ω_0) and view (Ω_v) directions, BRDFs $d_k(\Omega_0, \Omega_v)$ at N spectral bands and uncertainties $\delta_k(\Omega_0, \Omega_v)$ ($k = 1, 2, \dots, N$), find LAI and FPAR. The algorithm compares observed $d_k(\Omega_0, \Omega_v)$ and modeled $r_k(\Omega_0, \Omega_v, p)$ canopy reflectances for a suite of canopy structures and soil patterns that represent a range of expected natural conditions. Here p =[canopy, soil pattern] denotes a pattern of canopy structure and soil type (Kimes et al., 2000). All canopy/soil patterns p for which modeled and observed BRDFs differ by an amount equivalent to or less than the corresponding uncertainty, i.e.,

$$\frac{1}{N} \sum_{k=1}^N \left(\frac{r_k(\Omega_v, \Omega_0, p) - d_k(\Omega_v, \Omega_0)}{\delta_k} \right)^2 \leq 1, \quad (1)$$

are considered as acceptable solutions. FPAR is also calculated for each acceptable solution. The mean values of LAI and FPAR averaged over all acceptable solutions and their dispersions are taken as solutions and retrieval uncertainties (Knyazikhin et al., 1998b; Kimes, et al., 2000; Zhang et. al., 2000; Tian et. al., 2000). If the inverse problem has a unique solution for a given set of surface reflectances, mean LAI coincides with this solution and its dispersion equals zero. If Eq. (1) allows for multiple solutions, the algorithm provides a weighted mean in accordance with the frequency of occurrence of a given value of LAI. The dispersion magnitude indicates the reliability of the corresponding LAI value. The accuracy of retrievals can not be improved if no additional information is available. Figure 1 illustrates this approach. Note, the concept of multiple acceptable solutions was originally formulated and implemented in the MISR (Multi-angle Imaging SpectroRadiometer) aerosol retrieval algorithm (Martonchick et al., 1998).

In the case of a dense canopy, its reflectance in one or several directions can be insensitive to various parameter values (e.g., LAI) characterizing the canopy because, for example, the reflectance of solar radiation from the underlying soil surface or lower leaf-stories is completely obscured by the upper leaves (Price,1993; Liu and Huete, 1995; Jasinski, 1996; Carlson and Ripley, 1997). When this happens, the canopy reflectance is said to belong to the saturation domain (Knyazikhin et al., 1998b). The distribution of acceptable LAI values will appear flat over the range of LAI, illustrating that the solutions all have equal probability of occurrence (Fig. 1b). The reliability of LAI values retrieved under a condition of saturation is very low (Gobron et. al., 1997). This situation can be recognized by the retrieval technique (Knyazikhin et al., 1998b). We introduce a saturation index (SI) as

$$SI = \frac{\text{number of LAIs retrieved under conditions of saturation}}{\text{total number of retrieved LAI values}} .$$

This index is an indicator of the quality of the retrievals; that is, the smaller its value, the more reliable the algorithm output would be. One may expect low values of the saturation index when more information is used to retrieve LAI and FPAR (Diner et. al., 1999) However, the saturation index may increase with increase of uncertainties δ_k .

Given the set $\mathbf{d} = (d_1, d_2, \dots, d_N)$ of observed canopy reflectances, it may be the case that Eq. (1) has no solutions. A pixel for which the algorithm retrieves a value of LAI and FPAR is termed a retrieved pixel. The ratio of the number of retrieved pixels to the total number of processed pixels is the retrieval index (RI), i.e.,

$$\text{RI} = \frac{\text{number of retrieved pixels}}{\text{total number of vegetated pixels}} .$$

This variable characterizes the quality of LAI and FPAR maps showing of how the retrieved LAI and FPAR values cover the globe. It is a function of uncertainties in the observed and modeled canopy reflectances and number N of spectral bands used. Generally, the retrieval index increases with increasing uncertainties in data and model. However, increasing uncertainties means poor quality of input data and therefore poor quality in LAI/FPAR. Uncertainties, therefore, must be carefully evaluated in order to produce optimal algorithm performance. A better result should, in general, have a high retrieval index, low saturation index and retrieval dispersion.

UNCERTAINTIES IN MODELED AND OBSERVED CANOPY REFLECTANCES

Uncertainties in the land surface reflectance product and model uncertainties set a limit to the quality of retrievals and, thus, their specification is critical to production of global LAI and FPAR of maximum possible quality. Their definitions are presented in this section.

Uncertainties in the Land Surface Reflectance Product

Any satellite-borne sensor measures in-orbit radiances of the target through the atmosphere. Obtaining surface reflectances requires processing of the in-orbit data to correct for atmospheric and other environmental effects, which determines uncertainties in the surface reflectance product. Let d_1, d_2, \dots, d_N be atmospherically corrected BRDFs at N spectral bands. We treat these values as independent random variables with finite variances σ_k^2 , $k = 1, 2, \dots, N$, and

assume the deviations $\varepsilon_k=(d_k-m_k)/\sigma_k$ follow Gaussian distribution. Here m_k is the mathematical expectation of d_k , which are treated as “true values.” The random variable

$$\chi_{\sigma}^2[\mathbf{d} - \mathbf{m}] = \sum_{k=1}^N \varepsilon_k^2 = \sum_{k=1}^N \frac{(d_k - m_k)^2}{\sigma_k^2}, \quad (2)$$

characterizing the proximity of atmospherically corrected data $\mathbf{d} = (d_1, d_2, \dots, d_N)$ to true values $\mathbf{m} = (m_1, m_2, \dots, m_N)$ has a chi-square distribution. A value of $\chi_{\sigma}^2 \leq N$ indicates good accuracy in the atmospherically corrected surface reflectances. We assume that the atmospheric correction algorithm provides surface reflectances \mathbf{d} satisfying $\chi_{\sigma}^2 \leq N$ with a probability $1 - \alpha$; that is, $\text{Prob}(\chi_{\sigma}^2 > N) = \alpha$ where $1 - \alpha$ is the value of the chi-square distribution at N . Dispersions $\sigma = (\sigma_1, \sigma_2, \dots, \sigma_N)$ are uncertainties in the land surface reflectance product.

Model Uncertainty

Model uncertainty characterizes the accuracy of models to approximate natural variability, which in general is quite high. For example, consider two broadleaf forests (having the same canopy/soil patterns) located, say, in Siberia and in North America. The algorithm treats these as identical scenes. However, their reflectances can differ by 15-20% due to factors which were not accounted in the model. It means, one must assume 15-20% uncertainties in the simulation to account for the fact that these two forests are treated as belonging to one class. This type of uncertainties depend on the amount of information available when retrieving biophysical parameters from surface reflectances, as well as on the temporal and spatial resolution of data.

The propagation of model uncertainty through the retrieval technique starts when one replaces “true” reflectances \mathbf{m} in (2) with modeled reflectances $\mathbf{r} = (r_1, r_2, \dots, r_N)$. We use values $\varepsilon_{M,k} = (m_k - r_k) / \sigma_{M,k}$, to characterize the inaccuracy in model predictions. Dispersions $\boldsymbol{\sigma}_M = (\sigma_{M,1}, \sigma_{M,2}, \dots, \sigma_{M,N})$ are model uncertainties. Consider a canopy radiation model that can simulate surface reflectances \mathbf{m} with accuracy $\chi_{\sigma_M}^2[\mathbf{m} - \mathbf{r}] \leq N$. Based on the Minkowski inequality (Bronstein and Semengyaev, 1985), the following transformation of $\chi_{\sigma}[\mathbf{d} - \mathbf{r}]$ can be performed,

$$\begin{aligned} \chi_{\sigma}[\mathbf{d} - \mathbf{r}] &= \chi_{\sigma}[(\mathbf{d} - \mathbf{m}) - (\mathbf{r} - \mathbf{m})] \geq \left| \chi_{\sigma}[\mathbf{d} - \mathbf{m}] - \chi_{\sigma}[\mathbf{m} - \mathbf{r}] \right| \\ &= \left| \chi_{\sigma}[\mathbf{d} - \mathbf{m}] - \sqrt{\sum_{k=1}^N \frac{(m_k - r_k)^2}{\sigma_k^2}} \right| = \left| \chi_{\sigma}[\mathbf{d} - \mathbf{m}] - \sqrt{\sum_{k=1}^N \varepsilon_{M,k}^2 \frac{\sigma_{M,k}^2}{\sigma_k^2}} \right|. \end{aligned}$$

Thus, $\chi_{\sigma}[\mathbf{d} - \mathbf{r}]$ is a function of the ratio $\sigma_{M,k} / \sigma_k$. Let σ_k tends to zero (i.e., one has very accurate surface reflectance measurements) while holding $\sigma_{M,k}$ constant (i.e., the model is not improved).

The quantity $\chi_{\sigma}[\mathbf{d} - \mathbf{m}]$ is a bounded value, i.e., $\chi_{\sigma}[\mathbf{d} - \mathbf{m}] \leq \sqrt{N}$, while $\chi_{\sigma}[\mathbf{m} - \mathbf{r}]$ becomes arbitrary large. It means that the more accurately atmospheric correction is performed, the more inaccurately the solutions of Eq. (1) approximate LAI values in this case, because the “true” LAI values do not provide a good fit between observed and modeled reflectances. Ignoring the model uncertainty in the retrieval algorithm, therefore, causes a destabilization of the convergence process; that is, the more accurate the input information is, the more reliable the algorithm output should be. This instability also takes place when one uses the metric χ_{σ_M} characterizing the accuracy in model predictions without accounting for the uncertainties in measurements.

To stabilize the convergence process, a stabilized uncertainty $\boldsymbol{\delta} = (\delta_1, \delta_2, \dots, \delta_N)$ is introduced as $\delta_k^2 = (\sigma_{M,k}^2 + \sigma_k^2) / \theta^2$. Here θ is a stabilization parameter as specified below. This uncertainty is used to solve Eq. (1). It follows from the Minkowski inequality that

$$\begin{aligned} \chi_{\boldsymbol{\delta}}[\mathbf{d} - \mathbf{r}] &= \chi_{\boldsymbol{\delta}}[(\mathbf{d} - \mathbf{m}) + (\mathbf{m} - \mathbf{r})] \leq \chi_{\boldsymbol{\delta}}[\mathbf{d} - \mathbf{m}] + \chi_{\boldsymbol{\delta}}[\mathbf{m} - \mathbf{r}] \\ &= \sqrt{\sum_{k=1}^N \frac{(d_k - m_k)^2}{\sigma_k^2} \theta^2 \frac{\sigma_k^2}{\sigma_k^2 + \sigma_{M,k}^2}} + \sqrt{\sum_{k=1}^N \frac{(m_k - r_k)^2}{\sigma_{M,k}^2} \theta^2 \left(1 - \frac{\sigma_k^2}{\sigma_k^2 + \sigma_{M,k}^2}\right)} \\ &\leq \theta \lambda_{\max} \chi_{\boldsymbol{\sigma}}[\mathbf{d} - \mathbf{m}] + \theta (1 - \lambda_{\min}) \chi_{\boldsymbol{\sigma}_M}[\mathbf{m} - \mathbf{r}] \leq [\theta \lambda_{\max} + \theta (1 - \lambda_{\min})] \sqrt{N}, \end{aligned} \quad (3)$$

where

$$\lambda_{\max}^2 = \max_k \frac{\sigma_k^2}{\sigma_k^2 + \sigma_{M,k}^2}, \quad \lambda_{\min}^2 = \min_k \frac{\sigma_k^2}{\sigma_k^2 + \sigma_{M,k}^2}.$$

We assign a value to θ such that $\theta \lambda_{\max} + \theta (1 - \lambda_{\min}) = 1$ is satisfied, i.e., $\theta = 1 / (1 + \lambda_{\max} - \lambda_{\min})$. The stabilization parameter varies between 0.5 and 1. It follows from (3) that the use of the stabilized uncertainty establishes convergence of the retrieval technique; that is, tending σ_k and $\sigma_{M,k}$ to zero independently, “true” LAI always provides a good fit between observed and modeled reflectances within the stabilized uncertainty $\boldsymbol{\delta}$ and, thus, solutions of Eq. (1) can approximate the desired parameters.

The metric $\chi_{\boldsymbol{\delta}}$ is a decreasing function with respect to the stabilized uncertainty $\boldsymbol{\delta}$. If model and land surface product uncertainties are underestimated (i.e., $\boldsymbol{\delta} < \boldsymbol{\delta}_0$), the algorithm will not

admit those solutions of Eq. (1) which provide a good fit in the correct metric χ_{δ_0} and fail in the metric χ_{δ} . It can result in fewer solutions or even the absence of a solution to Eq. (1) and, consequently, in lower values of the dispersion and retrieval index. For example, all canopy/soil patterns with $\chi_{\delta_0}[\mathbf{d}-\mathbf{r}]=\sqrt{N}$, will be treated as unacceptable solutions in this case. The theory of ill-posed problems states that a best estimate of desired parameters satisfies $\chi_{\delta_0}[\mathbf{d}-\mathbf{r}]=\sqrt{N}$ (Tikhonov and Arsenin, 1986). Therefore, we cannot expect the decrease in the number of acceptable solutions, the dispersion and the retrieval index to indicate improvement in the algorithm output. On the contrary, the underestimation of real uncertainties can result in the deterioration of retrieval quality.

If model and land surface reflectance uncertainties are overestimated (i.e., $\delta > \delta_0$), then $\chi_{\delta}[\mathbf{d}-\mathbf{r}] \leq \chi_{\delta_0}[\mathbf{d}-\mathbf{r}] \leq \sqrt{N}$, i.e., the number of solutions to Eq. (1) and, consequently, the retrieval index will increase. It results in a larger number of acceptable solutions, higher retrieval index and, consequently, lower quality of LAI retrievals. Unlike the former case, however, the best estimation of the desired parameters satisfies Eq. (1). It means that the underestimation of uncertainties can result in a lower retrieval quality than their overestimation. A technique for modification of the algorithm for deriving biophysical parameters of the highest possible quality is equivalent to maximization of retrieval index, minimization of saturation index and the dispersion while holding the best estimation in the set of acceptable solutions. Accurate specification of uncertainties should provide a high value of retrieval index for any combination of spectral bands used in Eq. (1). Under this condition, the dispersion, retrieval index, and saturation index can characterize quality of retrievals.

To study the effect of uncertainties on retrievals, an overall uncertainty $\bar{\delta}$ is introduced as

$$\bar{\delta} = \sqrt[N]{\delta_1 \delta_2 \cdots \delta_N} ,$$

where δ_k is the stabilized uncertainty in the i th spectral band. The value of $\sqrt{N}\bar{\delta}^N$ is proportional to the area ($N=2$) or volume ($N>2$) of the ellipse/ellipsoid determined by the inequality (1) in the N -dimensional spectral space (Fig. 1a). In this paper, we will use a relative v_k and an overall relative $\bar{v}(N)$ uncertainty defined as

$$v_k = \frac{\delta_k}{r_k}, \quad k = 1, 2, \dots, N, \quad \bar{v}(N) = \sqrt[N]{v_1 v_2 \cdots v_N} . \quad (4)$$

The overall uncertainty can be considered as a measure of the uncertainty in model and land surface reflectance product. We cannot expect a lower uncertainty in the LAI/FPAR retrievals than the overall uncertainty. Two retrievals are said to be comparable if they were obtained from data having the same value of the overall uncertainty. On this equal-overall uncertainty basis, one can compare different retrievals as a function of the number N of spectral bands used to solve Eq. (1) and uncertainties $v_k, k = 1, 2, \dots, N$.

DATA ANALYSIS

Multispectral data from the Sea-Viewing Wide Field-of-view Sensor (SeaWiFS) were used to produce LAI/FPAR of the highest possible quality with the MODIS algorithm. Geocoded,

calibrated, cloud-screened and atmospherically corrected global surface reflectances in 8 spectral bands at 8km resolution were used in this study. The temporal range of data is September 1997, with nominal mission duration of 5 years. We used surface reflectances centered at 443 (blue), 555 (green), 670 (red) and 865 (near-infrared) nm to retrieve LAI and FPAR with MODIS algorithm (Knyazikhin et al., 1998a). The width of the blue, green and red bands was 20 nm, and NIR was 40 nm. For each pixel, solar and view zenith angles and azimuths were available and are required by the algorithm. The daily data of each month were composited into one layer based on the minimum-blue standard.

A biome Classification Map (BCM) is another important ancillary data layer used as input to the algorithm. The BCM is derived from the AVHRR Pathfinder data set (Myneni et. al. 1997). In this map, global vegetation is classified into 6 biome types: grasses and cereal crops, shrubs, broadleaf crops, savannas, broadleaf forests and needle forests. The structural attributes of these biomes are parameterized in terms of variables that the radiative transfer model admits (Myneni et al., 1997). The three-dimensional transport equation was used to simulate canopy reflectances r_k , $k = 1, 2, \dots, N$, using the BCM, sun-view geometry and canopy/soil pattern as input (Knyazikhin et al., 1998a).

Spectral Signature of the SeaWiFS Surface Reflectances

Figure 2 presents histograms of canopy reflectances for different spectral bands and biome types and Table 1 shows mean values of these histograms. Typically, global canopy reflectance varies between 0 and 0.2 at the red band, 0.1 and 0.4 at the NIR band, 0 and 0.15 at the green band and less than 0.1 at the blue band. On average, needle forests have the strongest absorption in red,

green and blue bands, but have a stronger reflectance in the NIR band. Grasses can be regarded as the “brightest” biome exhibiting almost the highest reflectances in red, green and blue bands. Broadleaf crops have a strong reflectance in both NIR and red bands while the reflectance of broadleaf forests is strong in NIR but very low in the red band.

The Normalized Difference Vegetation Index (NDVI) is defined as $(d_{\text{NIR}} - d_{\text{R}})/(d_{\text{NIR}} + d_{\text{R}})$, where d_{NIR} and d_{R} are observed reflectances at the NIR and red band, respectively. The NDVI is a very important measure of chlorophyll abundance and energy absorption. The histograms of NDVI values derived from the SeaWiFS data in July and November 1998 are shown in Fig. 3c and 3d. Most of the broadleaf and needle forests exhibit very high NDVI values compared to other biomes. On average, the mean values are 0.67 for broadleaf and 0.71 for needle forests, respectively (Table 1).

It is helpful to introduce a data density function that indicates how densely the pixels occupy the spectral space. Each point in the N -dimensional spectral space represents reflectances $\mathbf{d} = (d_1, d_2, \dots, d_N)$ of a pixel at N spectral bands. The data density function is defined as the number of points per unit volume about the point \mathbf{d} . Figs. 3a, 3b and 4 demonstrate 25% data density contours in different two-dimensional spectral spaces. Each contour separates an area on the spectral plane of high data density containing 25% of the pixels from a given biome type. These contours show the most probable location of pixels belonging to a given biome type in the spectral space. The better these contours are separated, the more distinguishable the corresponding biomes are. In the red–NIR plane (Figs. 3a and 3b) grasses and crops are well separated from forests. In between these are broadleaf crops and savannas. Both biomes have high NDVI and their contours are close to the NIR axis. The NDVI of grasses and cereal crops is substantially lower and their contours are close to the soil line. Figure 4 shows that contours can

overlap, especially in the red–blue plane. The degree of overlap depends on resolution of the data (Tian et al., 2000). The contours are maximally separated in the red–NIR plane. This indicates that these two bands contain maximum information about the biome type, at least, in the case of 8 km resolution data. This may explain why the algorithm produces reasonable results when using red and NIR data only.

Figure 3 demonstrates seasonal variation in the contour location and NDVI distribution. All contours move toward the soil line from July (Fig. 3a) to November (Fig. 3b) because of a decrease in LAI. This shift is more pronounced in the case of shrubs. The area of the contours becomes larger in November, which implies a lower data density. The NDVI distributions also show a sharp seasonal change (Figs. 3c and 3d).

QUALITY OF LAI/FPAR RETRIEVALS

Monthly minimum–blue composite SeaWiFS reflectances over the vegetated areas in July and November 1998 were chosen as input to the algorithm in this section. The term vegetated pixel is used to refer to pixels of NDVI value greater than 0.1. The algorithm was run pixelwise over all vegetated pixels. In this section, we discuss performance of the algorithm as a function of the number of spectral bands and overall uncertainties.

The relative uncertainties (Eq. 4) are input to the LAI/FPAR algorithm. However, the SeaWiFS processing does not provide this information routinely. Therefore, we start with the estimation of a possible upper boundary of the overall uncertainty $\bar{v}(N)$ as follows. Assuming that the relative uncertainties in red, v_R , and NIR, v_{NIR} , reflectances are wavelength independent, i.e., $v_R = v_{NIR} = \bar{v}(2)$, find such $\bar{v}(2)$ for which 95% of all land pixels for which Eq. (1) has no

solutions for non-vegetated areas and corrupted data due to clouds or atmospheric effect. SeaWiFS surface reflectances at red and NIR spectral bands ($N=2$) acquired over land on September 22 were used to specify $\bar{v}(2)$. The solution to this problem was $\bar{v}(2)=0.2$ (Knyazikhin et al., 1998c; Kimes et al., 2000). This value was assigned to $\bar{v}(N)$. Thus, this upper level of the overall uncertainty allows the algorithm to discriminate between vegetation and non-vegetation reflectances.

The uncertainties in the land surface reflectance product can be estimated from the atmospheric correction algorithm (Vermote et al., 1997; Kaufman et al., 1997). Table 2 shows a theoretical estimate of the relative uncertainties in the MODIS surface reflectance product (Vermote, 2000). The following values were assigned to the relative uncertainties (4) in our study, $v_R = 0.2$ (red), $v_{NIR} = 0.05$ (NIR), $v_B = 0.8$ (blue), and $v_G = 0.1$ (green). The overall relative uncertainty $\bar{v}(4)$ of the four spectral bands is 0.168, which is quite close to the upper boundary of the overall uncertainty specified above.

To investigate the quality of the LAI/FPAR fields retrieved from multi-spectral surface reflectances (multi-band retrieval), we ran the algorithm using the composite SeaWiFS surface reflectances with (1) two (red and NIR); (2) three (red, NIR and green); and (3) four (red, NIR, green, and blue) spectral bands as input. The objective of this section was to analyze the use of different combinations of spectral bands to produce LAI and FPAR fields. Special emphasis was given to assessing the influence of relative uncertainties on the quality of the retrieved LAI/FPAR product.

Multiband Retrieval with Band Independent Uncertainties

It is assumed in this subsection that the relative uncertainties (Eq. 4) do not depend on wavelength, i.e., $\nu_R = \nu_{NIR} = \nu_B = \nu_G$, each being set to upper level of the overall uncertainty 0.2. Figure 5 shows the retrieval index for various biome types and number of the input spectral bands used. For a certain uncertainty setting, the retrieval index is a decreasing function of the number of bands. One can see a sharp jump caused by inclusion of the blue surface reflectance in Eq. (1). Table 3 summarizes the use of different combinations of spectral bands in the retrieval technique. All combinations of spectral bands exclude the blue, on average, have higher values of retrieval index. The following arguments can be presented. The foliage optical properties at blue and red wavelengths are similar and, thus, the canopy reflectances at these spectral bands are comparable in magnitude. However, atmospheric effect at blue is much stronger than at red and, therefore, uncertainties in the atmospherically corrected surface reflectances are greater at blue than at red band (Table 2). However, these were set to 0.2, i.e., the stabilized uncertainty appears to be substantially underestimated and the retrieval index decreased.

Dispersions of retrieved LAI values for two biome types and various combinations of input spectral bands are shown in Fig. 6. Although some minor differences exist, one can not see much improvement in the retrieval quality when the number N of bands used to retrieve LAI and FPAR increases. The saturation index for different combinations of spectral bands is summarized in Table 4. It is only slightly sensitive to N . This implies that we can not improve accuracy in retrievals by simply including more spectral bands.

Multiband Retrieval with Band Dependent Uncertainties

Including more spectral information in the retrieval technique initiates two competing processes: increase of information content of data and decrease of overall accuracy in the input data. The first enhances the quality of retrievals, while the second suppresses it. In this subsection, we set values of relative uncertainties to the uncertainties in the land surface reflectance product (Table 2) which are treated as the lower bound of the overall uncertainties. It should be noted that the model uncertainty in canopy reflectance at the green spectral band can be quite high. Indeed, leaf albedo at this wavelength is characterized by temporal variation. For example, a young leaf reflects more energy than an old one. This was not accounted in our model and, thus, the relative uncertainty at the green wavelength is probably underestimated.

Figure 7 demonstrates the accuracy of retrieved LAI values derived from surface reflectances at red and NIR wavelengths ($N=2$, legends “R&NIR,bd” and “R&NIR,bi”), and at red, NIR and green ($N=3$; legends “R&NIR&G,bd” and “R&NIR&G,bi”) spectral bands. Abbreviation “bd” (band dependent) and “bi” (band independent) identify two cases. In the first case, the relative uncertainties v_k depend on wavelength (Table 2). In the second case, relative uncertainties are wavelength independent, each being set to $\bar{v}(N) = \sqrt[N]{v_1 v_2 \cdots v_N}$, $N=2$ or 3. Note that in all cases, the overall uncertainty $\bar{v}(N)$ has the same value (0.1). Again, retrieval dispersions are slightly sensitive to the number N of input spectral bands. However, their values are clearly lower compared to those shown in Fig. 6. This indicates that the retrieval dispersion is sensitive to the overall uncertainty but not to the number N of spectral bands in Eq. (1), i.e., retrieval accuracy is mainly determined by uncertainties in input data. Figure 8 shows the retrieval index for the four cases described above. The overall uncertainty affects the retrieval

index; that is, retrieval index increases with increase of the overall uncertainty (compare Figs. 5 and 8). However, with overall uncertainty constant, an accurate prescription of band-dependent uncertainties results in higher values of the retrieval index (Fig. 8).

Table 5 shows the saturation index for different biomes and number N ($N = 2, 3$ and 4) of input spectral bands. Values of relative uncertainties listed in Table 2 were taken as input for Eqs. (1) and (4). First of all, the saturation index decreased compared to those shown in Table 4, i.e., accurate surface reflectance data and models provide higher quality retrievals. Note that the saturation index is a decreasing function of N (Table 5), and when the overall uncertainty $\bar{v}(N)$ increases from 0.1 ($N = 2$ and 3) to 0.168 ($N = 4$), the saturation index has not increased. Therefore, an increase in the overall uncertainty due to more input spectral bands does not necessarily suppress the increase in information supplied to the algorithm if accurate band-specific uncertainties are available.

Figure 9 demonstrates the retrieval index for $N = 4$ (four band retrieval) as a function of biome type and overall uncertainties. The bars labeled “0.1,” “0.168,” “0.2” correspond to the cases when relative uncertainties in spectral reflectances were wavelength independent, i.e. $v_k = \bar{v}(4)$, and set to 0.1, 0.168 and 0.2, respectively. The legend “0.168bd” identifies retrieval indices obtained by using band-specific uncertainties v_k (Table 2). One can see that the use of band specific uncertainties results in higher retrieval index, and retrievals of the best possible quality.

Test of Physics

It is well known that there is a strong relationship between a vegetation index, such as NDVI, and surface parameters such as LAI and FPAR (Asrar et. al., 1984; Tucker and Sellers, 1986; Peterson et. al. 1987; Verma et. al. 1993; Myneni and Williams, 1994; Chen, 1996). This relationship provides a method to test the physics of retrievals. Figure 10 shows the NDVI-LAI and NDVI-FPAR regression curves for two biome types derived using the retrieved LAI and FPAR fields and NDVI computed from SeaWiFS surface reflectances. These correspond to literature reports (Myneni et al., 1997; Clevers, 1989). Note that the LAI values were retrieved directly from surface spectral reflectances without using the NDVI. The advantages of using spectral reflectance rather than NDVI are: a) NDVI/LAI relations are sensitive to changes in sun angle, view angle and background reflectance, while the MODIS algorithm actually exploits these changes to retrieve LAI. b) the NDVI based algorithm can use two spectral bands only, while Eq. (1) can ingest all the available spectral information to improve quality of the retrievals. It should be noted that the retrieved LAI and FPAR fields regressed against SeaWiFS NDVI shown in Fig. 10 were obtained using different combinations of spectral bands as input to Eq. (1). Irrespective of the number of input bands, the NDVI/LAI and NDVI/FPAR relations appear to be close to each other within an accuracy determined by the overall uncertainty $\bar{v}(N)$. This illustrates algorithm consistence with respect to the physical processes responsible for the observed variation in canopy spectral reflectances.

SEAWIFS LAI/FPAR GLOBAL PRODUCT

With the above results as guiding principles, we now discuss global LAI/FPAR fields derived from monthly SeaWiFS data from January, April, July and October. Surface reflectances at red, NIR and green bands and band-dependent uncertainties listed in Table 2 were used to produce these fields. When the algorithm failed to retrieve a LAI value, the NDVI–LAI and NDVI–FPAR regression curves shown in Fig. 10 were used to estimate LAI and FPAR values. This is similar to the processing for MODIS data.

Histograms of LAI values for the four months are shown in Fig. 11. For comparison, a ten-year average global LAI distributions derived from the AVHRR pathfinder 8 km data using a NDVI based algorithm (Myneni et al., 1997) is also shown in Fig. 11. The histograms clearly show the seasonal variations. Shrubs and needle forests located in the northern hemisphere have low LAI values in the winter (Fig. 11a). During the boreal summer, their LAI increases (Fig. 11e). Savannas in the southern hemisphere have minimum LAI values in the dry period during July (Fig. 11e). Broadleaf forests which are located in both the northern and southern hemispheres have a bimodal distribution of LAI

Figures 12 and 13 are color-coded images of SeaWiFS LAI and FPAR fields for the four months, in 1998. In the northern hemisphere, LAI increases from January to a maximum in July and then decreases towards October. On contrary, because January and April are wet and July is dry season in Africa, LAI values have the lowest values in July. This is consistent with Fig. 11.

CONCLUSIONS

In this paper, we examine the quality of LAI and FPAR fields derived from SeaWiFS multispectral surface reflectances using the MODIS LAI/FPAR algorithm as a function of input and model uncertainties. When the amount of spectral information input to the LAI/FPAR algorithm is increased, not only does this increase the overall information content but also decreases the summary accuracy in data. The former enhances the quality of retrievals, while the latter suppresses it. The total uncertainty sets a limit on the quality of the retrieved fields. Accurate specification of the uncertainties of inputs to the algorithm is critical to production of global biophysical variables, and to realize the basic principle of any retrieval technique; that is, the more the measured information and the more accurate this information is, the more reliable and accurate the algorithm output will be. This approach was used to produce global SeaWiFS LAI/FPAR fields of the highest possible quality. Comparing with published results shows this approach works reasonably well.

ACKNOWLEDGMENTS

This research was carried out jointly by personnel at Boston University and NASA GSFC under contract with the National Aeronautic and Space Administration.

REFERENCES

- Asrar, G., Fuchs, M., Kanemasu, E. T., and Harfield, J. L. (1984), Estimating absorbed photosynthetic radiation and leaf area index from spectral reflectance in wheat. *Agron. J.*, 76:300-306.
- Bronstein, I. N., and Semendyayev, K. A. (1985), *Handbook of Mathematics*, Springer, Berlin, 973 pp.
- Carlson, T. N., and Ripley, D. A. (1997), On the relation between NDVI, fractional vegetation cover, and leaf area index. *Remote Sens. Environ.*, 62:241-252.
- Chen, J. M. (1996), Canopy architecture and remote sensing of the fraction of photosynthetically active radiation absorbed by boreal conifer forests. *IEEE Trans. Geosci. Remote Sens.*, 34:1353-1368.
- Clevers, J. G. P. W. (1989), The application of a weighted infrared-red vegetation index for estimating leaf area index by correcting for soil moisture. *Remote Sens. Environ.*, 29:25-37.
- Deschamps, P.Y., Bréon, F.M., Leroy, M., Podaire, A., Bricaud, A., Buriez, J.C., and Sèze, G. (1994), The POLDER mission: Instrument characteristics and scientific objectives, *IEEE Trans. Geosci. Remote Sens.*, GE-32:598-615.
- Diner, D. J., Asner, G. P., Davies, R., Knyazikhin, Y., Muller, J.P., Nolin, A. W., Pinty, B., Schaaf, C. B., and Stroeve, J. (1999), New directions in Earth observing: Scientific application of multi-angle remote sensing. *Bulletin of the American Meteorological Society*, 80:2209-2228.

- Gobron, N., Pinty, B. and Verstraete, M. M. (1997), Theoretical limits to the estimation of leaf area index on the basis of visible and near-infrared remote sensing data. *IEEE Trans. Geosci. Remote Sens.*, 35:1438-1445.
- Jasinski, M. F. (1996), Estimation of subpixel vegetation density of natural regions using satellite multispectral imagery. *IEEE Trans. Geosci. Remote Sens.*, 34:804-813.
- Justice, O., Vermote, E., Townshend, J.R.G., et al. (1998), The moderate resolution imaging spectroradiometer (MODIS): Land remote sensing for global research, *IEEE Trans. Geosci. Remote Sens.*, 36, 4:1228-1249.
- Kaufman, Y. J., Tanre, D., Remer, L., Vermote, E. F., Chu, A., and Holben, B. N. (1997), Operational remote sensing of tropospheric aerosol over the land from EOS-MODIS. *J. Geophys. Res.*, 102(14):170351-17068.
- Kimes, D., Knyazikhin, Y., Privette, J., Abuelgasim, A., and Gao, F. (2000), Inversion methods for physically-based models. *Remote Sensing Reviews* (in print).
- Knyazikhin, Y., Martonchik, J. V., Myneni, R. B., Diner, D. J., and Runing, S. (1998a), Synergistic algorithm for estimating vegetation canopy leaf area index and fraction of absorbed photosynthetically active radiation from MODIS and MISR data. *J. Geophys. Res.*, 103:32257-32275.
- Knyazikhin, Y., Martonchik, J. V., Diner, D. J., Myneni, R. B., Verstraete, M., Pinty, B. and Gobron, N. (1998b), Estimation of vegetation canopy leaf area index and fraction of absorbed photosynthetically active radiation from atmosphere-corrected MISR data. *J. Geophys. Res.*, 103:32239-32256.

- Knyazikhin, J., Zhang, Y., Yian, Y., Shabanov, N., and Myneni, R. (1998c), Radiative transfer based synergistic MODIS/MISR algorithm for the estimation of global LAI&FPAR. MODIS quarterly report: Jan/01/98–Mar/31/98, NASA, Greenbelt, MD.
- Kuusik, A. (1985), The hot-spot effect of a uniform vegetative cover, *Sov. J. Remote. Sens.*, 3:645–658.
- Liu, Q., and Huete, A. (1995), A feedback based modification of the NDVI to minimize canopy background and atmospheric noise. *IEEE Trans. Geosci. Remote Sens.*, 33:457-465.
- Martonchik, J.V., Diner, D.J., Kahn, R., Ackerman, T. P., Verstraete, M. M., Pinty, B., and Gorbon, H. R. (1998), Techniques for the retrieval of aerosol properties over land and ocean using multiangle imaging, *IEEE Trans. Geosci. Remote Sens.*, 36:1212-1227.
- Myneni, R. B., and Williams, D. L. (1994), On the relationship between FAPAR and NDVI. *Remote Sens. Environ.*, 49:200-211.
- Myneni, R. B., Nemani, R. R., and Running, S. W. (1997), Estimation of global leaf area index and absorbed PAR using radiative transfer models. *IEEE Trans. Geosci. Remote Sens.*, 35:1380-1393.
- Myneni, R.B. (1991), Modeling radiative transfer and photosynthesis in three-dimensional vegetation canopies. *Agric. For. Meteorol.*, 55:323-344.
- Peterson, D. L., Spanner, M. A., Running, R. W., and Band, L. (1987), Relationship of thematic mapper simulator data to leaf area index. *Remote Sens. Environ.*, 22:323-341.
- Price, J. C. (1993), Estimating leaf area index from satellite data. *Remote Sens. Environ.*, 31:727-734.

- Ross, J., Knyazikhin, Y., Kuusk, A., Marshak, A., and Nilson, T. (1992), *Mathematical Modeling of the Solar Radiation Transfer in Plant Canopies* (in Russian, with English abstract), Gidrometeoizdat, St. Peterburg, Russia 195 pp.
- Ross, J.K., and Marshak, A. L. (1984), Calculation of the solar radiation reflection from plant cover using the Monte-Carlo method, *Sov. J. Remote. Sens.*, 5:58-67.
- Sellers, P. J., Los, S. O., Tucker, C. J., Justice, C. O., Dazlich, D. A., Collatz, G. J., and Randall, D. A. (1996), A revised land surface parameterization (SiB2) for atmospheric GCMs: II. The generation of global field fields of terrestrial biophysical parameters from satellite data. *J. Climate*, 9(4):706-737.
- Sellers, P. J., Randall D. A., Betts A. K., Hall F. G., Berry J. A., Collatz G. J., Denning A. S., Mooney H. A., Nobre C. A., Sato N., Field C. B., Henderson-sellers A.. (1997), Modeling the exchanges of energy, water, and carbon between continents and the atmosphere. *Science*, 275:502-509.
- Tian, Y., Zhang, Y., Knyazikhin, Y., Myneni, R.B., Glassy, J.M., Dedieu, D., and Running, S.W. (2000), Prototyping of MODIS LAI and FPAR algorithm with LASUR and LANDSAT data. *IEEE Trans. Geosci. Remote Sens.*, 38(5):2387-2401.
- Tikhonov, A.N., and Arsenin, V. Y. (1986), *Methods for Solving Ill-Posed Problems* (in Russian), Nauka, Moscow, 288 pp.
- Tucker, C. J., and Sellers, P. J. (1986), Satellite remote sensing of primary production. *Int. J. Remote Sens.*, 7:1395-1416.
- Verma, S. B., Sellers, P. J., Walthall, C. L., Hall, F. G., Kim, J., and Goetz, S. J. (1993), Photosynthesis and stomatal conductance related to reflectance on the canopy scale. *Remote Sens. Environ.*, 44:103-116.

- Vermote, E. (2000), Product accuracy/Uncertainty: MOD09, surface reflectance; atmospheric correction algorithm product. In MODIS Data Products Catalog (EOS AM Platform), <http://modarch.gsfc.nasa.gov/MODIS/RESULTS/DATAPROD/>.
- Vermote, E. F., Ei Saleous, N. Z., Justice, C. O., Kaufman, Y. J., Privette, J., Remer, L., Roger, J. C., and Tanre, D. (1997), Atmospheric correction of visible to middle infrared EOS-MODIS data over land surface, background, operational algorithm and validation. *J. Geophys. Res.*, 102(14):17131-17141.
- Verstraete M.M., Pinty, B., and Dickenson, R.E. (1990), A physical model of the bidirectional reflectance of vegetation canopies. 1. Theory, *J. Geophys. Res.*, 95:11765-11775.
- Zhang, Y., Tian, Y., Knyazikhin, Y., Martonchick, J. V., Diner, D. J., Leroy, M. and Myneni, R. B. (2000), Prototyping of MISR LAI and FPAR algorithm with POLDER data over Africa, *IEEE Trans. Geosci. Remote Sens.*, 38(5):2402-2418.

Table 1. Mean reflectance of various biome types

Spectral Band	Biome					
	Grass/Cereal Crops	Shrubs	Broadleaf Crops	Savannas	Broadleaf Forests	Needle Forests
Red	0.104	0.087	0.081	0.083	0.058	0.042
NIR	0.244	0.227	0.288	0.245	0.286	0.255
Blue	0.049	0.038	0.048	0.050	0.047	0.027
Green	0.090	0.078	0.086	0.082	0.073	0.059
NDVI	0.409	0.477	0.559	0.503	0.670	0.713

Table 2. Theoretical estimation of relative uncertainties in atmospherically corrected surface reflectances (Vermote, 2000)

Spectral Band	1 (Red)	2 (NIR)	3 (Blue)	4 (Green)
Center of Band, nm	670	865	443	555
Bandwidth, nm	20	40	20	20
Relative Error, %	10-33	3-6	50-80	5-12
v_k , dimensionless	0.2	0.05	0.8	0.1

Table 3. Retrieval index for various combinations of spectral bands used to retrieve LAI and FPAR in the case of band independent uncertainties, $\bar{v}(N)=0.2$

Spectral Bands Used				Biome Type					
Red	NIR	Blue	Green	Grasses/Cereal Crops	Shrubs	Broadleaf Crops	Savannas	Broadleaf Forests	Needle Forests
√	√			0.970	0.978	0.897	0.972	0.386	0.666
√	√		√	0.941	0.923	0.843	0.962	0.37	0.573
√			√	0.936	0.909	0.867	0.973	0.719	0.714
√	√	√	√	0.717	0.72	0.685	0.648	0.274	0.395
√		√		0.648	0.697	0.744	0.548	0.634	0.76
√	√	√		0.651	0.708	0.671	0.572	0.267	0.47
		√	√	0.893	0.74	0.808	0.876	0.713	0.513

Table 4. Saturation Index for various combinations of spectral bands used to retrieve LAI and FPAR in the case of band independent uncertainties, $\bar{v}(N) = 0.2$

Spectral Bands Used				Biome Type					
Red	NIR	Blue	Green	Grasses/Cereal crops, %	Shrubs, %	Broadleaf Crops, %	Savannas, %	Broadleaf Forests, %	Needle Forests, %
√	√			13.0	5.8	16.9	10.3	62.2	49.5
√	√		√	13.0	3.7	11.3	10.6	60.3	44.7
√	√	√	√	12.2	3.9	10.6	11.4	60.5	43.3

Table 5. Saturation Index for various combinations of spectral bands used to retrieve LAI and FPAR in the case of band dependent uncertainties determined in Table 2

Spectral Bands Used				Uncertainty, $\bar{v}(N)$	Biome Type					
Red	NIR	Blue	Green		Grasses/Cereal Crops, %	Shrubs, %	Broadleaf Crops, %	Savannas, %	Broadleaf Forests, %	Needle Forests, %
√	√			0.1	8.6	1.4	15.1	8.4	48.8	21.4
√	√		√	0.1	6.5	0.2	6.2	8.9	44.1	9.55
√	√	√	√	0.168	6.3	0.2	5.5	8.0	43.8	10.2

Table Captions

Table 1. Mean reflectance of various biome types

Table 2. Theoretical estimation of uncertainties in atmospherically corrected surface reflectances (Vermote, 2000)

Table 3. Retrieval index for various combinations of spectral bands used to retrieve LAI and FPAR in the case of band independent uncertainties, $\bar{v}(N) = 0.2$

Table 4. Saturation Index for various combinations of spectral bands used to retrieve LAI and FPAR in the case of band independent uncertainties, $\bar{v}(N) = 0.2$

Table 5. Saturation Index for various combinations of spectral bands used to retrieve LAI and FPAR in the case of band dependent uncertainties determined in Table 2

Figure Captions

Figure 1. (a) Distribution of processed pixels with respect to their reflectances at red (d_{RED}) and near infrared (d_{NIR}) spectral bands derived from SeaWiFS data (September 22, 1997). Inequality (1), $N=2$, defines an ellipse with the semi-axes $\sqrt{2} \delta_{\text{RED}}$ and $\sqrt{2} \delta_{\text{NIR}}$ centered at the point $(d_{\text{RED}}, d_{\text{NIR}})$. Each canopy/soil pattern for which modeled reflectances belong to the ellipse is an acceptable solution. For each set $\mathbf{d} = (d_{\text{RED}}, d_{\text{NIR}})$ of observed spectral reflectances one sorts the set of acceptable solutions into ascending order with respect to LAI values and defines a solution distribution function $\Phi_{\delta}(l, \mathbf{d})$ as the portion of different LAI values which are less than l . (b) Solution density distribution function $d\Phi_{\delta}(l, \mathbf{d})/dl$ for five different pixels. Mean LAI over this distribution and its dispersion are taken as LAI retrieval and its uncertainty, respectively.

Figure 2. Histograms of SeaWiFS canopy reflectances in July 1998: (a) red spectral band; (b) near infrared spectral band; (c) green spectral band; and (d) blue spectral band.

Figure 3. Statistical properties of SeaWiFS canopy reflectances. Distribution of pixels with respect to their reflectances at red and near infrared spectral bands in (a) July 1998 and (b) November 1997. Each biome dependent contour identifies an area of high data density that contains 25% of the pixels from a given biome type. NDVI histograms for six biome types in (c) July 1998 and (d) November 1997.

Figure 4. 25% density contours in (a) red–green; (b) red–blue; (c) green–NIR; and (d) in blue–NIR spectral spaces.

Figure 5. Retrieval index for various biome types and spectral bands used to produce LAIs. R&NIR: red and near infrared bands; R&NIR&G: red, near infrared, and green bands; R&NIR&B&G: red, near infrared, blue, and green bands. Relative uncertainties were set to the upper bound 0.2.

Figure 6. Dispersions DLAI and DFPAR of retrieved LAI and FPAR values for two biome types (grasses and cereal crops; broadleaf forests) and spectral bands used by the algorithm. The meaning of the labels R&NIR, R&NIR&G, and R&NIR&B&G is the same as in Figure 5. Relative uncertainties were set to the upper bound 0.2.

Figure 7. Dispersions DLAI and DFPAR of retrieved LAI and FPAR values for two biome types (grasses and cereal crops; broadleaf forests) derived from SeaWiFS surface reflectances at red and NIR (label R&NIR); red, NIR and green (label R&NIR&G) spectral bands. Abbreviators “bd” (band dependent) and “bi” (band independent) identify two cases, namely, “bd:” the relative uncertainties depend on wavelength whose values are presented in Table 2; “bi:” the relative uncertainties are wavelength independent, each being set to 0.1.

Figure 8. Retrieval index for various biome types and spectral bands used to produce LAIs. Labels have the same meaning as in Figure 7.

Figure 9. Retrieval index for various biome types and relative uncertainties derived from SeaWiFS surface reflectances at red, near infrared, green and blue spectral bands. The bars labeled “0.1”, “0.168,” and “0.2” correspond to the cases when relative uncertainties in spectral reflectances were wavelength independent and set to 0.1, 0.168 and 0.2, respectively. The label “0.168bd” identifies retrieval indexes obtained by using band-specific uncertainties presented in Table 2.

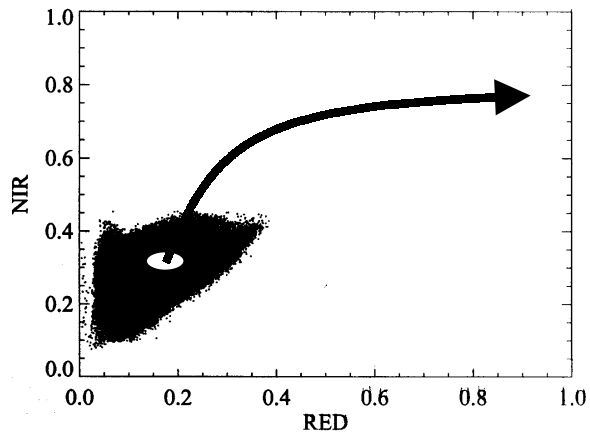
Figure 10. NDVI–LAI and NDVI–FPAR regression curves for two biome types (grasses and cereal crops; broadleaf forests). LAI and FPAR fields were derived from SeaWiFS surface reflectances at red and near infrared (label N&NIR) and red, near infrared and green (label R&NIR&G) spectral bands which then were regressed against SeaWiFS NDVI. Relative uncertainties listed in Table 2 were used.

Figure 11. Seasonal variation of LAI histograms derived from the MODIS LAI/FPAR algorithm with SeaWiFS surface reflectances (right column) and NDVI based algorithm (Myneni et al., 1997) with 10-year averaged Pathfinder data (right column).

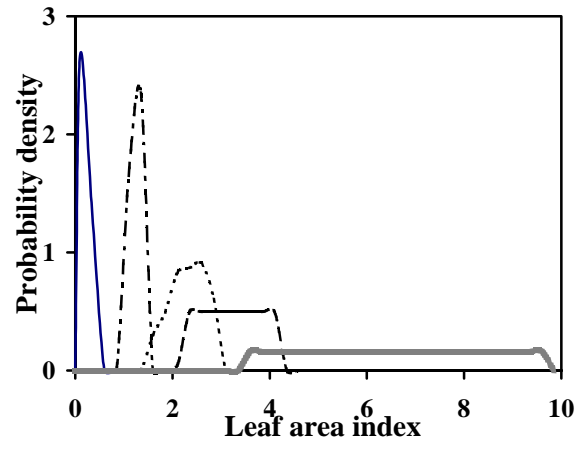
Figure 12. SeaWiFS global LAI in January, April, July and October, 1998.

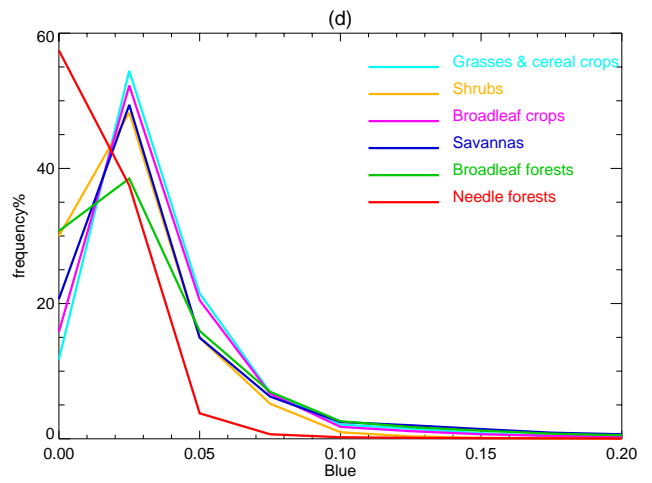
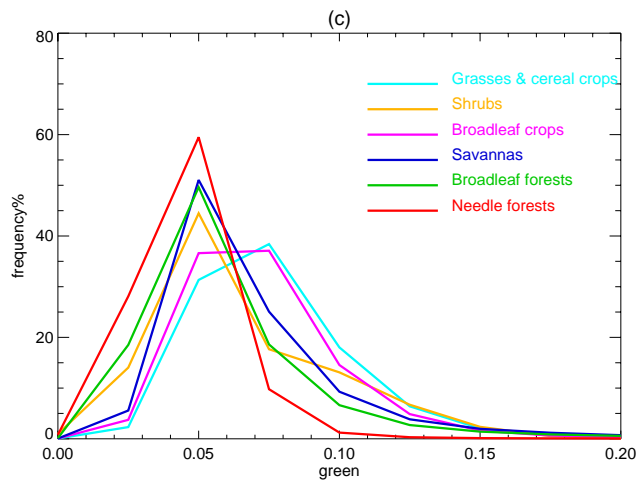
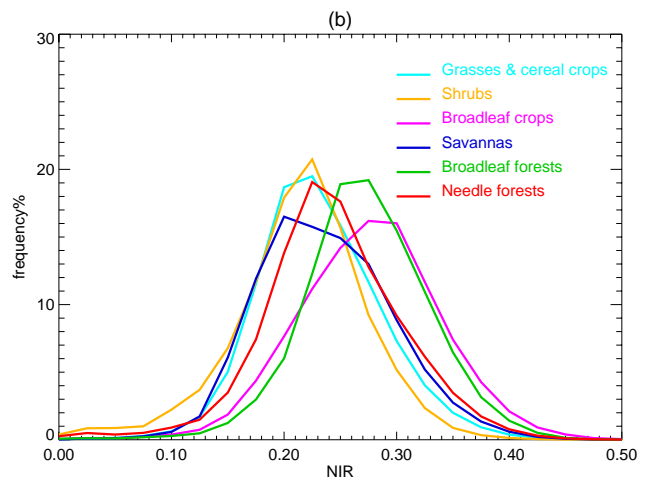
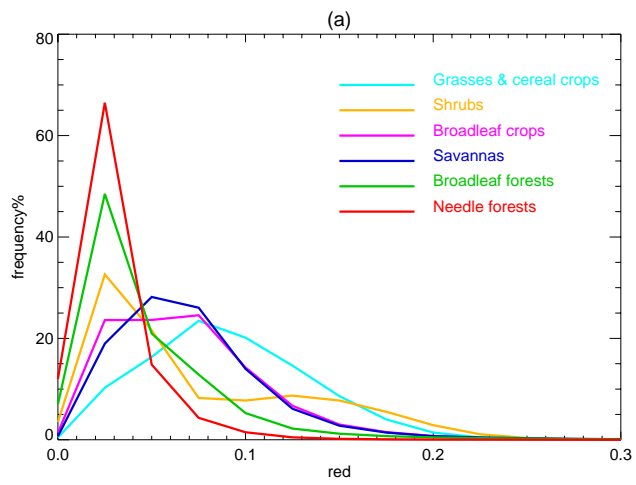
Figure 13. SeaWiFS global FPAR in January, April, July and October, 1998.

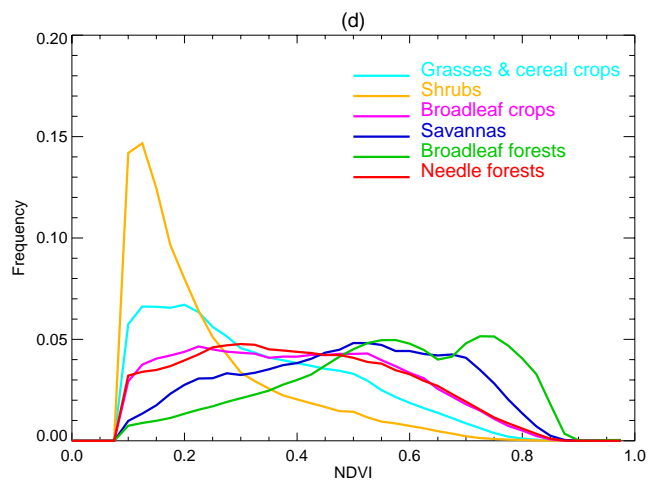
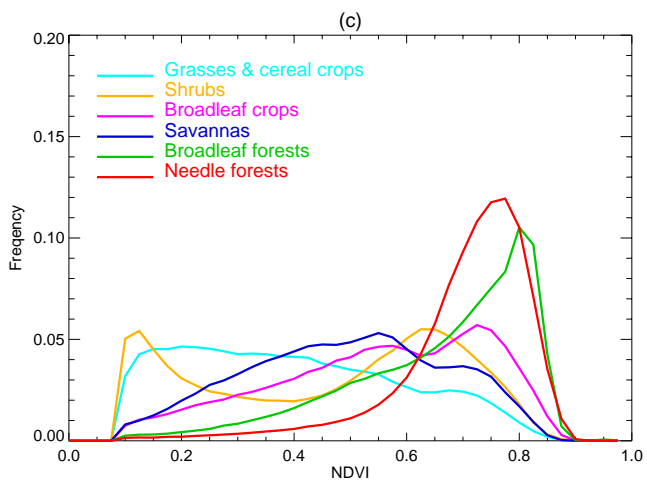
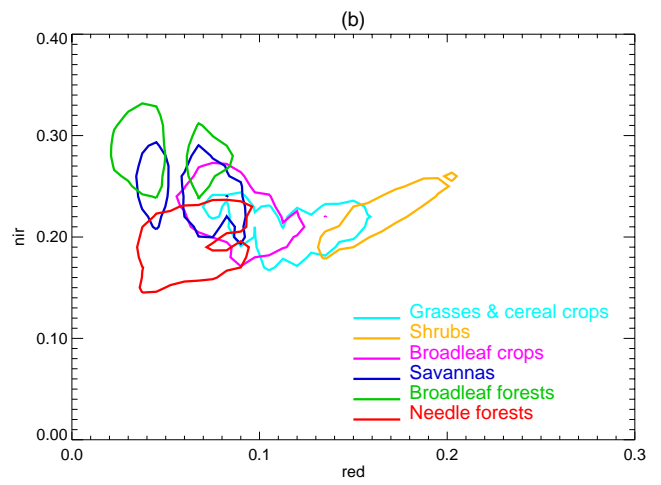
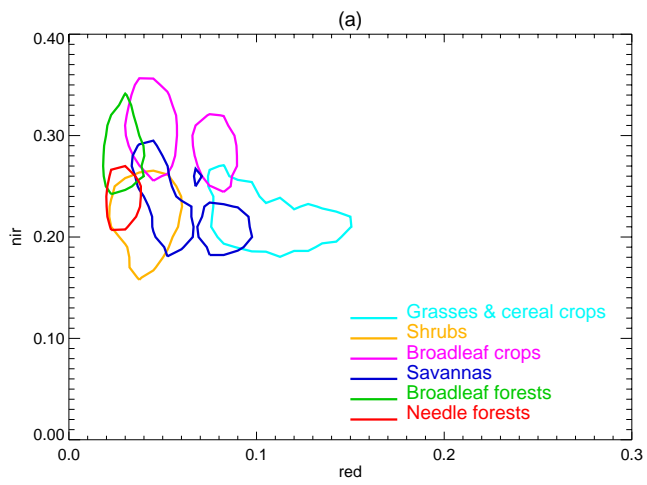
(a)

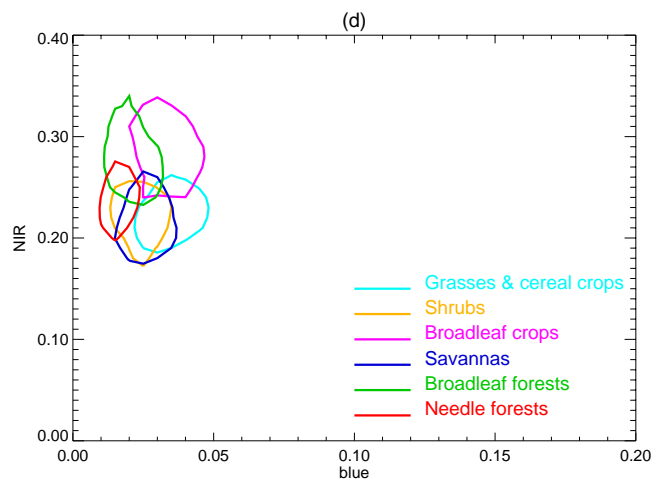
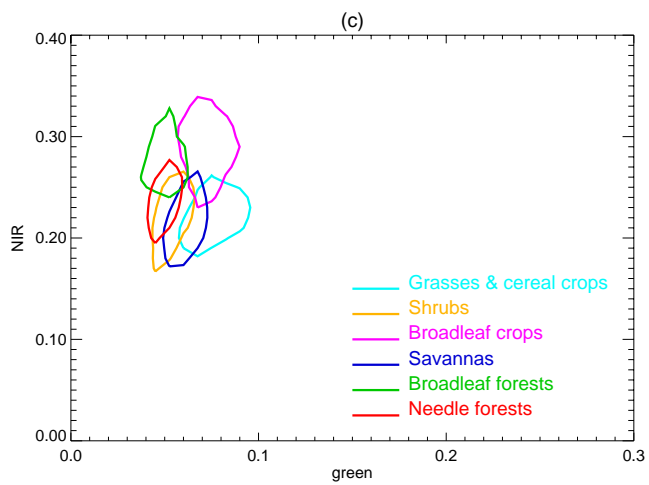
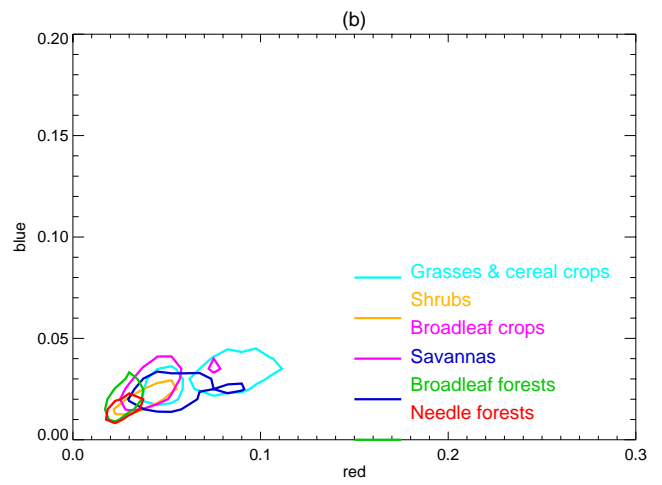
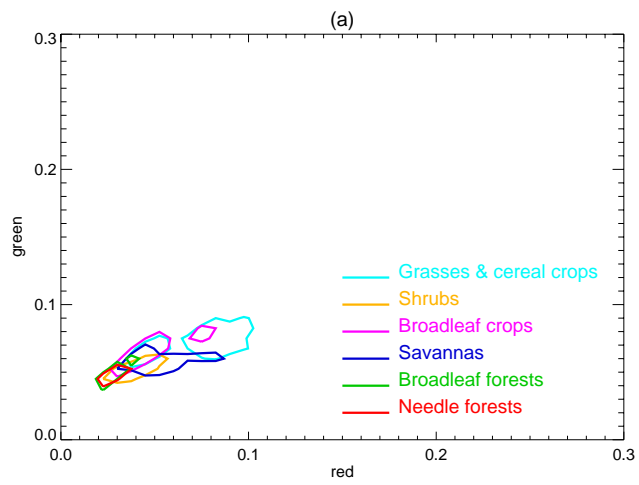


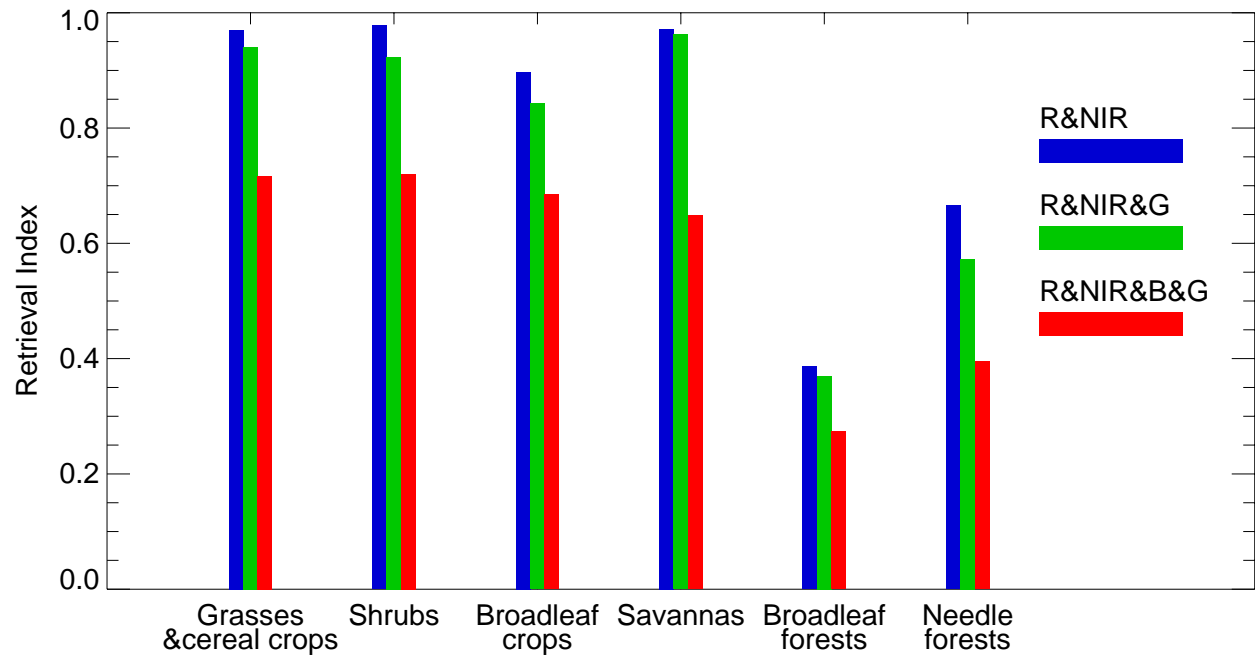
(b)

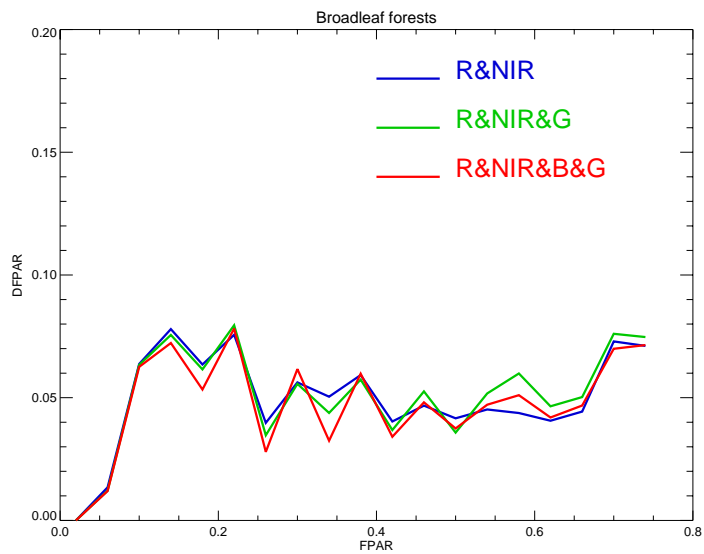
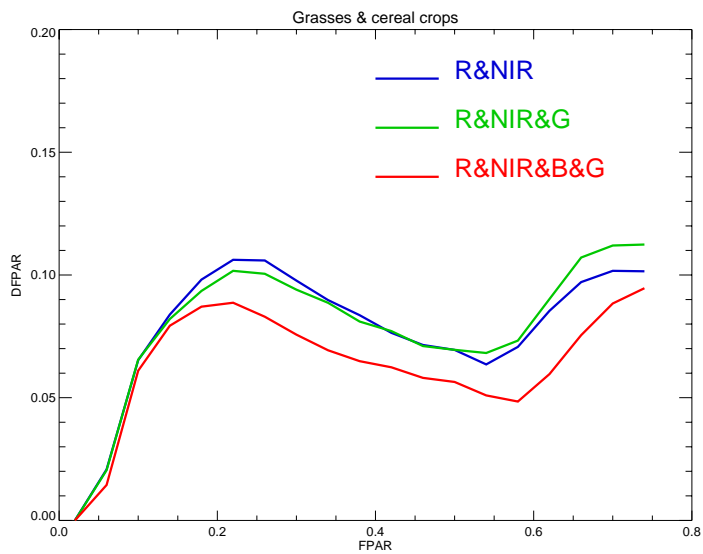
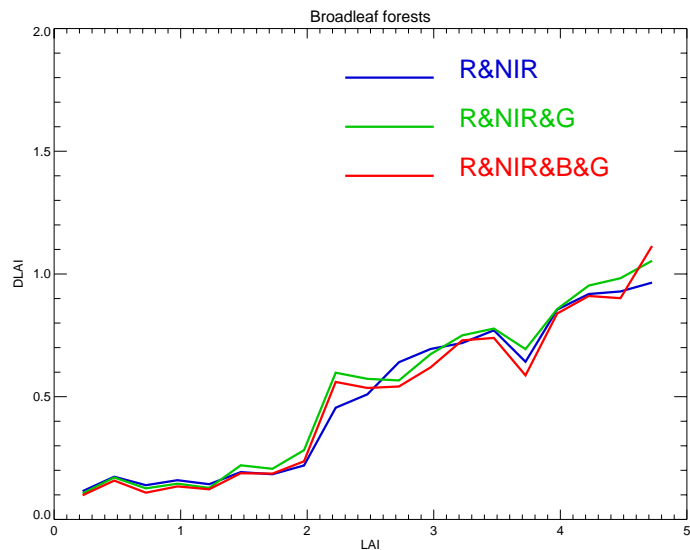
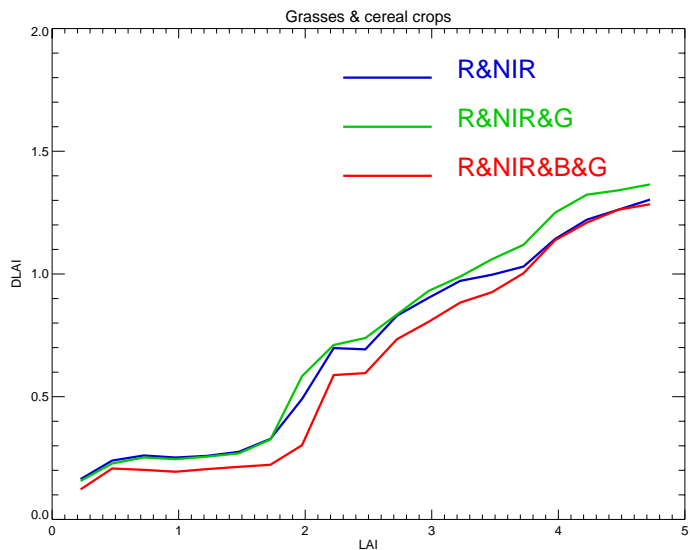


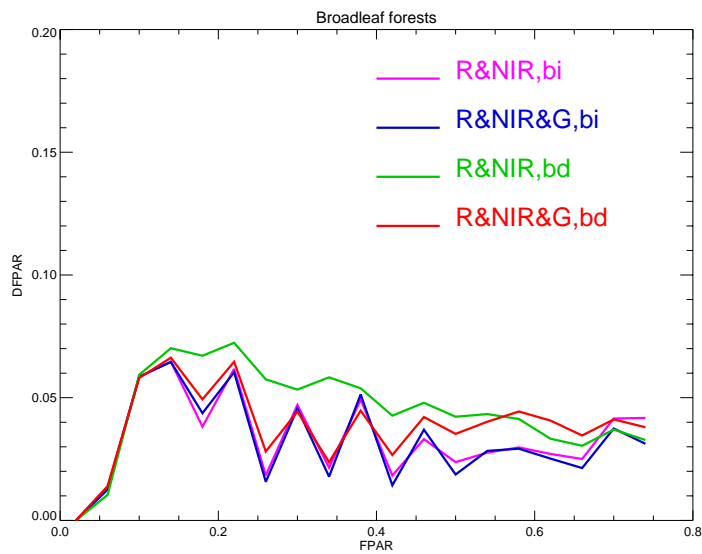
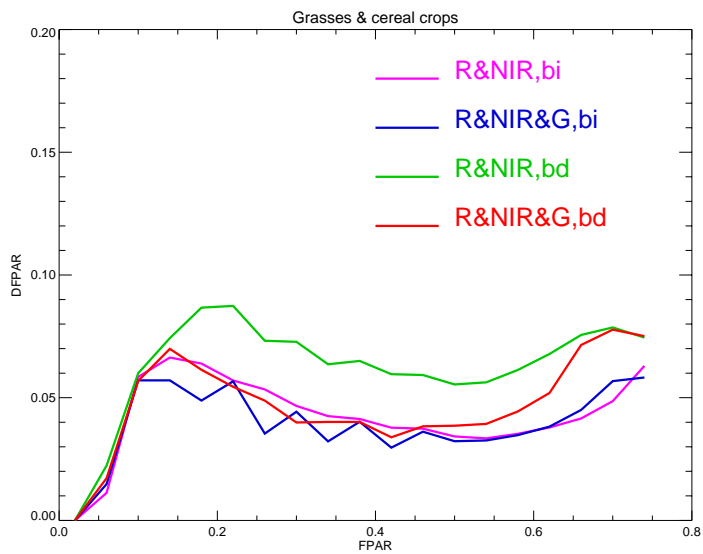
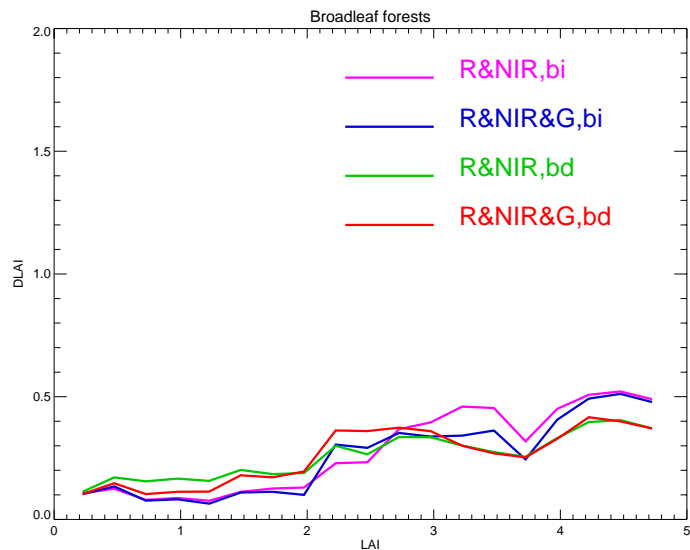
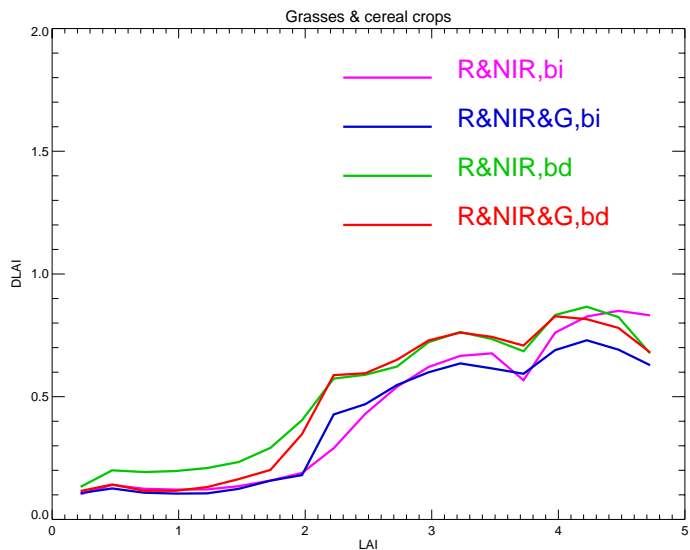


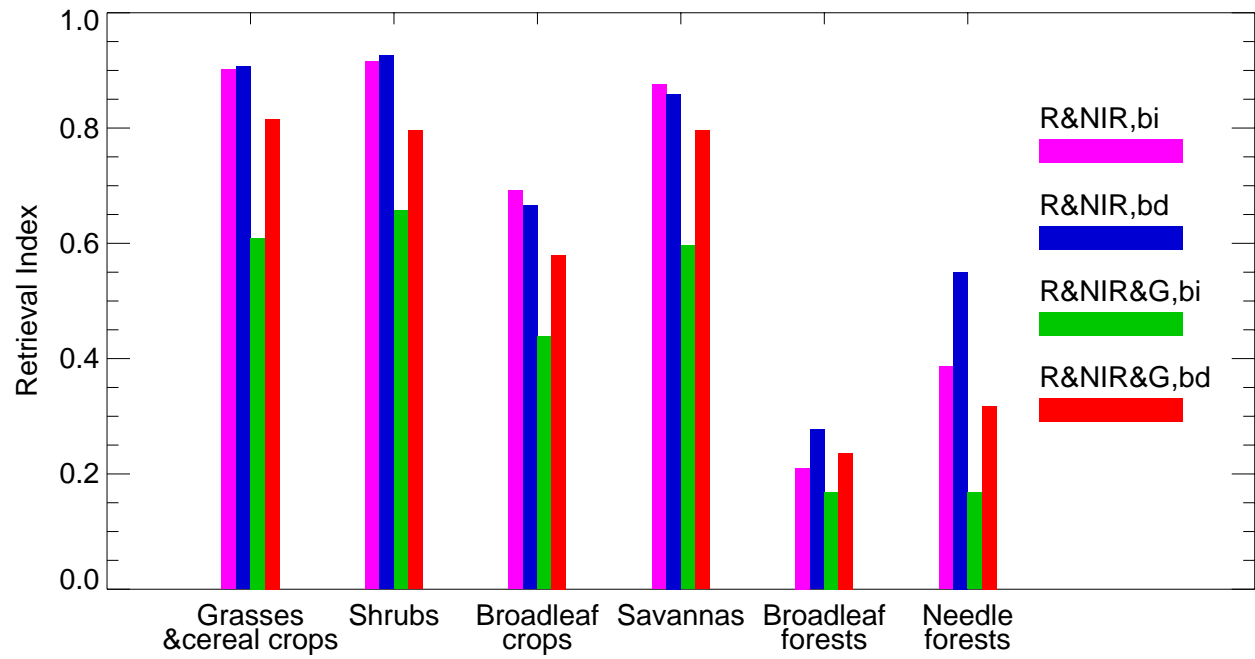


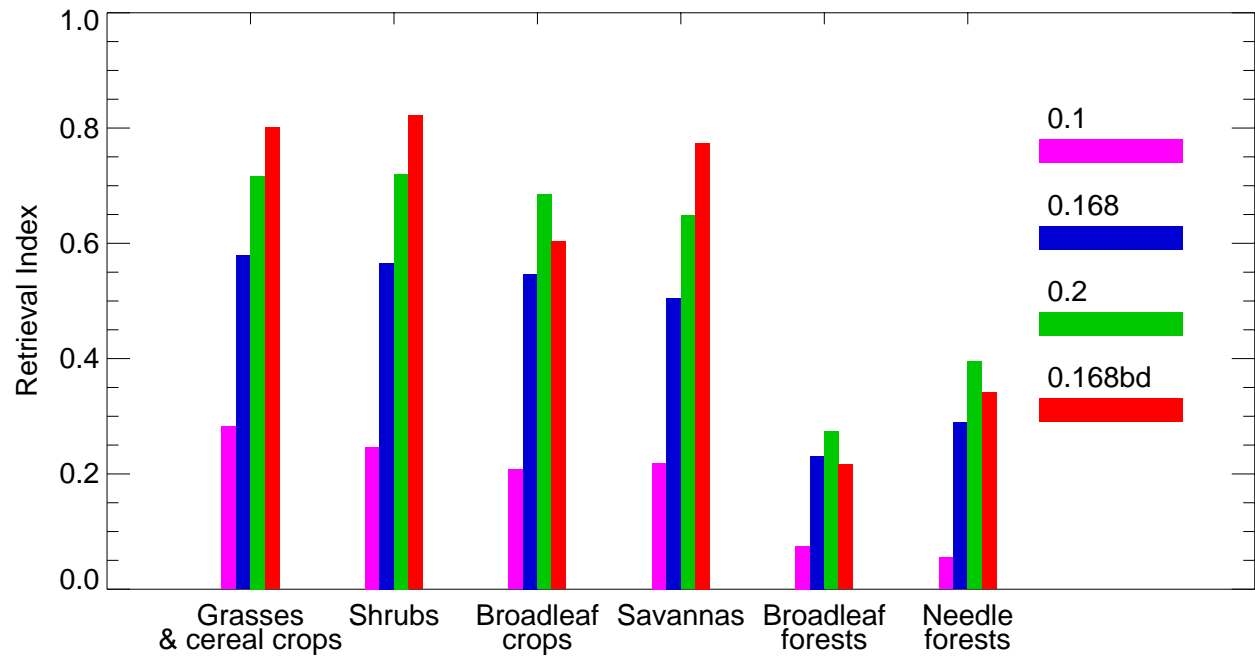


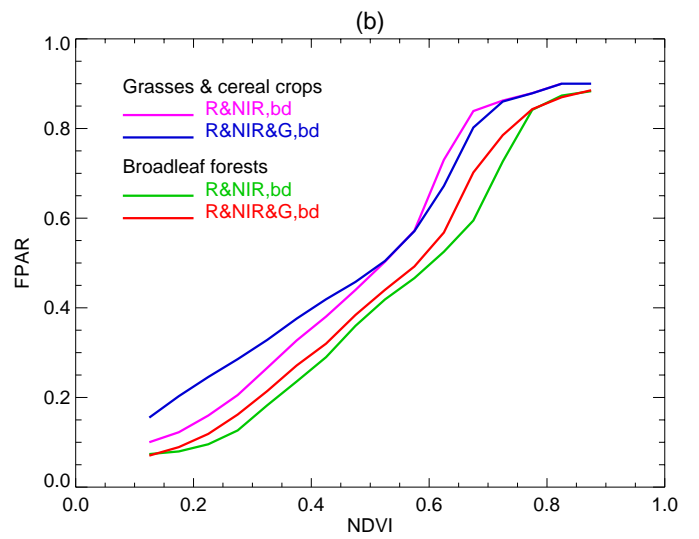
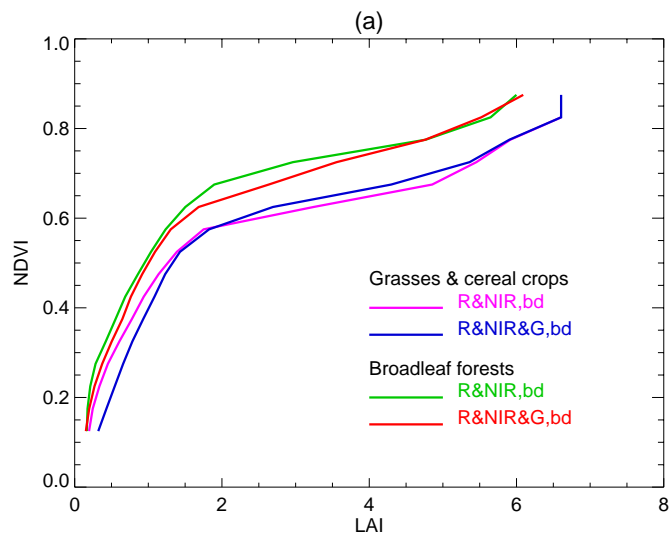


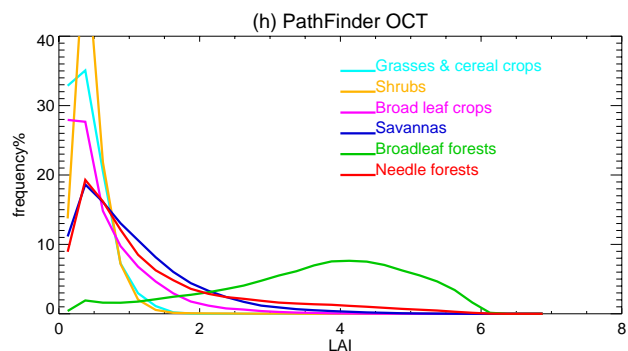
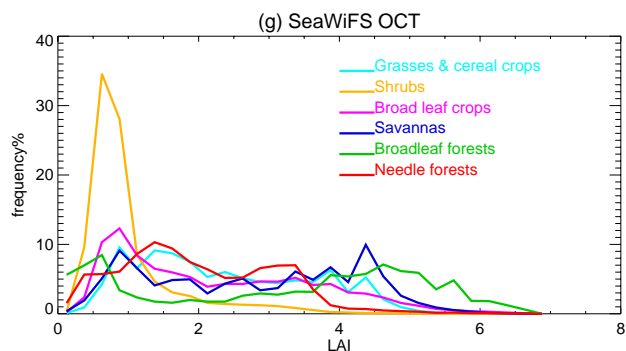
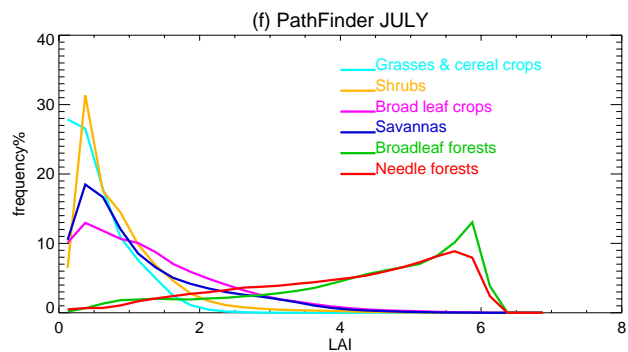
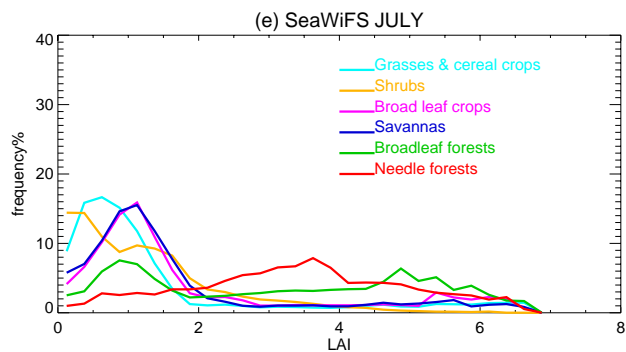
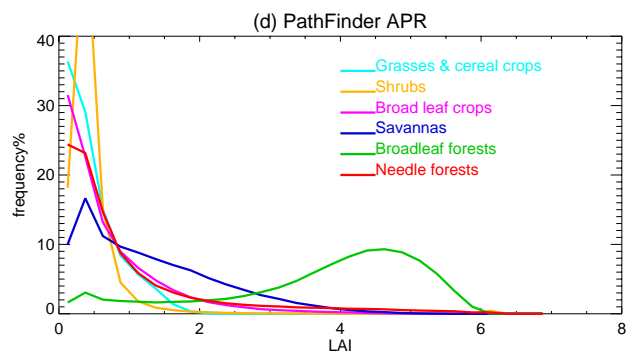
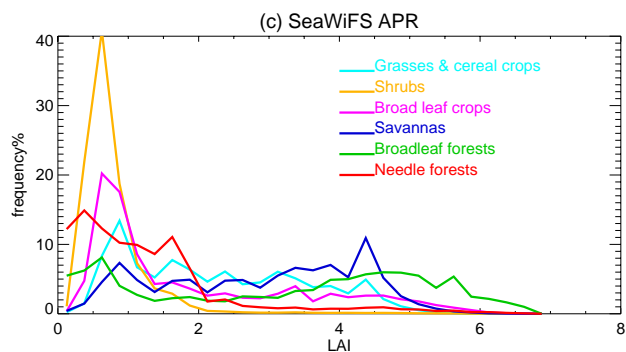
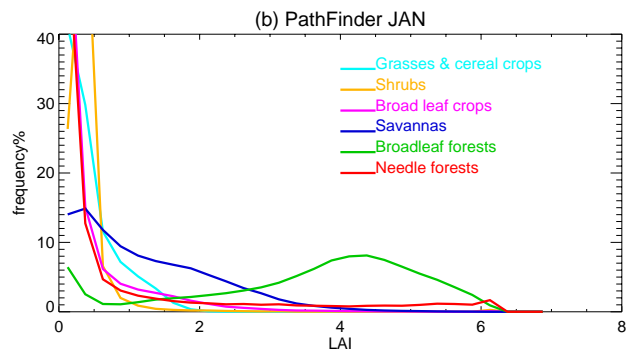
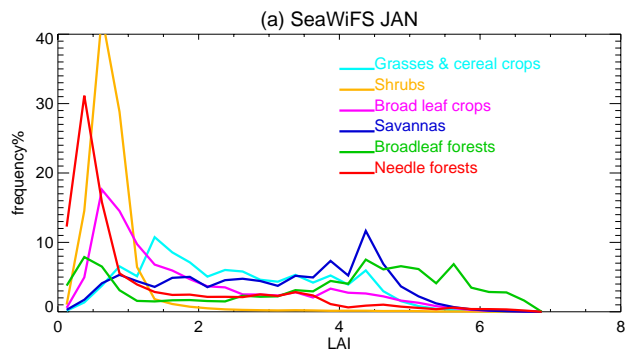


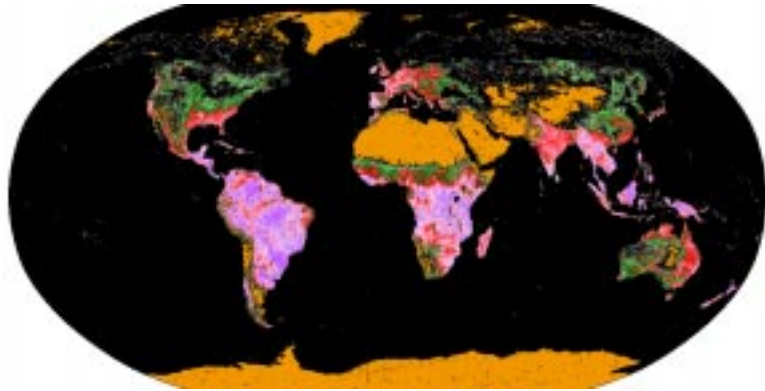




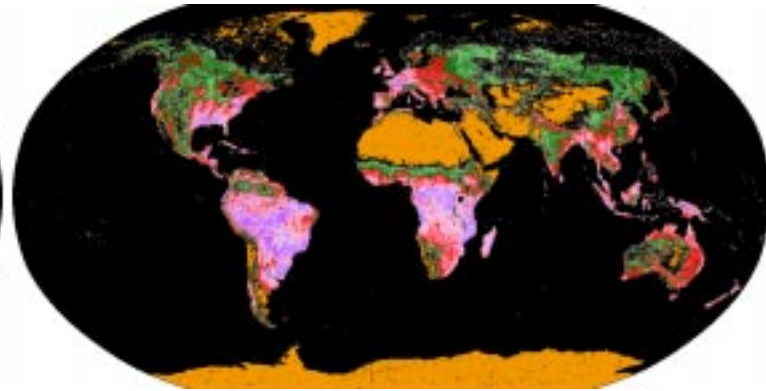




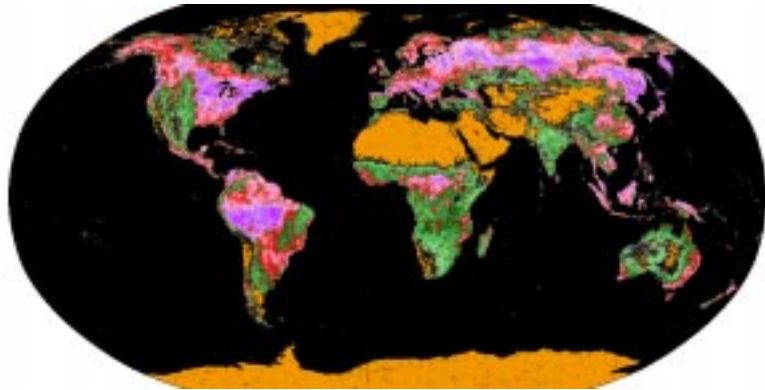




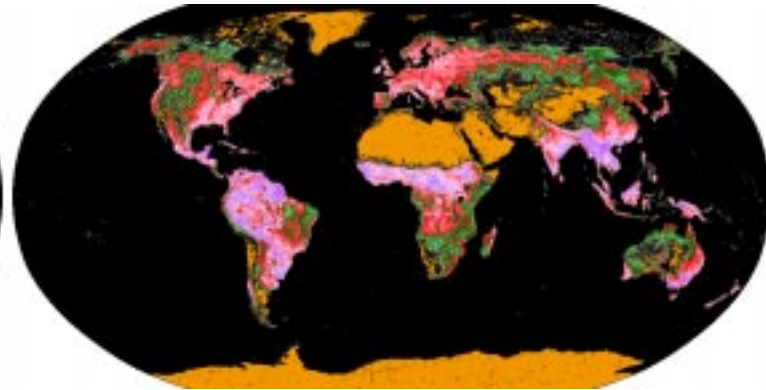
January



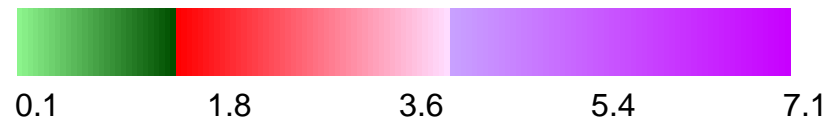
April

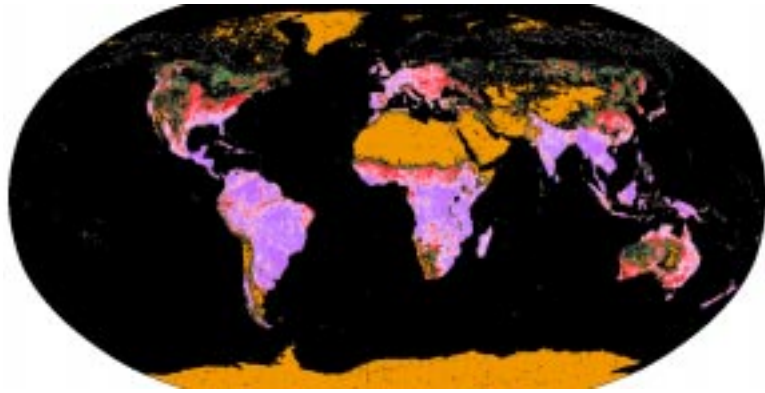


July

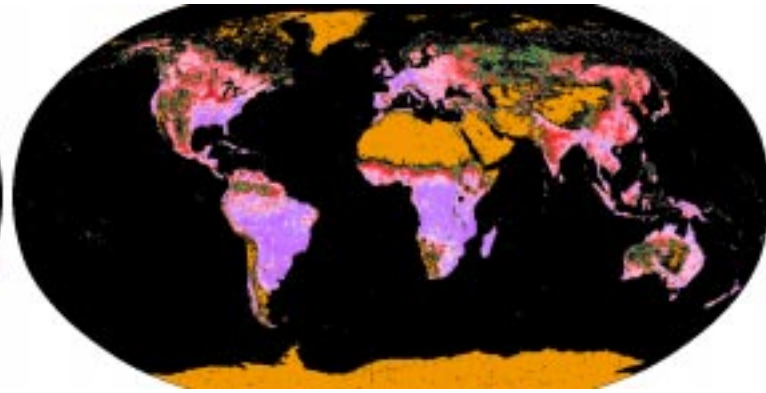


October

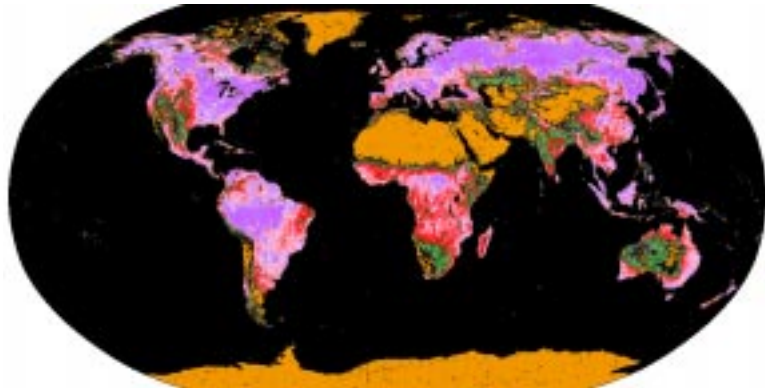




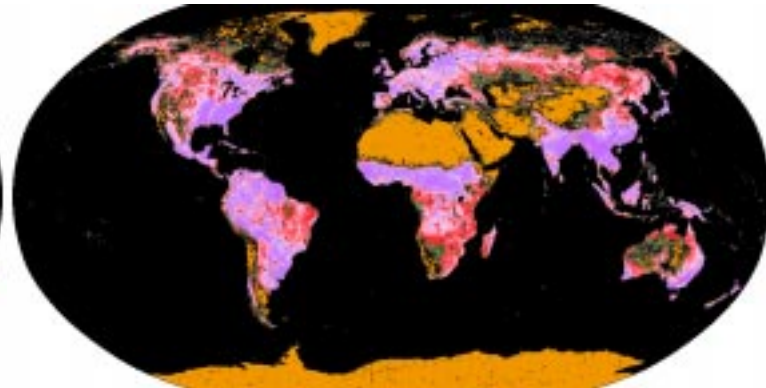
January



April



July



October

